Research Square

Preprints are preliminary reports that have not undergone peer review.
They should not be considered conclusive, used to inform clinical practice,
or referenced by the media as validated information.

RUL Prediction of Lithium-Ion Batteries Using VMD and a Multiscale TCN

Zhengjun Huang
Jinhua University of Vocational Technology
Tengfei Xiang
tfxiang@yeah.net

Zhejiang Technical Institute of Economics
Zhenzhen Qu
Jinhua University of Vocational Technology

Article

Keywords: lithium-ion battery, remaining useful life, fusion method, variational modal decomposition, multiscale temporal convolutional network

Posted Date: March 24th, 2026

DOI: https://doi.org/10.21203/rs.3.rs-9077622/v1

License: This work is licensed under a Creative Commons Attribution 4.0 International License.
Read Full License

Additional Declarations: No competing interests reported.

RUL PREDICTION OF LITHIUM-ION BATTERIES USING VMD AND A MULTISCALE TCN

Zhengjun Huang[1], Tengfei Xiang[2]*, Zhenzhen Qu[1]

1. Aeronautical Engineering College, Jinhua University of Vocational Technology, Jinhua 321017, China
2. Automotive technology college, Zhejiang Technical Institute of Economics, Hangzhou 310018,China
**correspond:* tfxiang@yeah.net

ABSTRACT

Accurate prediction of the remaining useful life (RUL) of lithium-ion batteries mitigates overuse risks, provides decision-making support for the secondary utilization of retired batteries, and enhances their second-life value. To address the impact of nonlinear characteristics caused by noise and capacity recovery phenomena on the accuracy of RUL prediction, this paper proposes a joint method based on variational mode decomposition (VMD) and a multiscale temporal convolutional network (TCN). First, the raw battery capacity data was decomposed using VMD, which separated the nonlinear degradation characteristics into high-frequency components and the primary degradation trend into low-frequency components. Second, for the high-frequency components, rolling iterative forecasting with a multiscale TCN was employed to capture short-term capacity variations. For the low-frequency components, features extracted from operational data were fed into the multiscale TCN to capture long-term capacity trends. Finally, the predictions from both components were integrated to reconstruct the capacity forecast. Validation results on NASA datasets demonstrate that the proposed method achieves a minimum root mean square error (RMSE) of 0.0104 and a corresponding mean absolute error (MAE) of 0.0084 for capacity prediction. The RUL prediction error is largely confined to within one cycle, indicating the method's excellent prediction capability.

Keywords: lithium-ion battery, remaining useful life, fusion method, variational modal decomposition, multiscale temporal convolutional network

1. INTRODUCTION

The performance of lithium-ion batteries deteriorates over time due to the aging of internal components and operating conditions[1,2]. Accurately predicting the remaining useful life (RUL) is therefore crucial for extending battery service life, mitigating performance degradation risks, and ensuring reliable management of electric vehicle power systems[3-5].

RUL prediction has become a prominent research focus in the field of fault prediction and health management for lithium-ion power batteries[6,7]. Existing RUL prediction methods primarily fall into two categories: model-based approaches and data-driven methods[8-10]. Model-based methods aim to establish mathematical models that describe battery degradation behavior to predict future performance, with their accuracy heavily reliant on the precision of the model[11,12]. For instance, Khodadadi et al.[13] employed an electrochemical model to extract features related to capacity degradation for RUL prediction under various operating conditions. However, such methods often involve high computational complexity and require substantial specialized knowledge. Similarly, Bin et al.[14] utilized a real-time rainflow counting algorithm to construct an aging mechanism model for real-time state-of-health (SOH) estimation. A key limitation of this approach is its strong dependence on specific battery manufacturing processes and materials, which restricts its general applicability. In another study, Liang et al.[15] integrated an empirical aging model with a mechanism model to achieve accurate life prediction for electric vehicle batteries. Nevertheless, the model's complexity, challenging parameter identification, and significant computational demands remain considerable obstacles. While Zhang et al.[16] proposed an improved unscented particle filter method with linear optimization-based resampling to mitigate particle diversity loss, their approach still struggles to fully resolve the issue of particle degeneracy.

Compared with model-driven approaches, data-driven methods do not require knowledge of the electrochemical

mechanisms of lithium-ion batteries and demonstrate greater adaptability[17,18]. Wang et al.[19] achieved joint SOH and RUL prediction using Gaussian process regression (GPR) and least squares support vector machines (LSSVM). However, this method is highly susceptible to outliers, as both the battery capacity recovery phenomenon and outliers can significantly affect prediction results. Wu et al.[20]employed the PF-LSTM model to predict the RUL of lithium-ion batteries. Although this model effectively handles complex nonlinear relationships, it fails to address the inherent long-term dependency issues of LSTM. Dong et al.[21] proposed a RUL prediction method for lithium-ion batteries that integrates singular value decomposition (SVD), stacked autoencoders (SAE), and Gaussian process regression (GPR). This approach effectively improved prediction accuracy but neglected the coupling relationships among battery capacity health indicators.

Owing to the nonlinear characteristics and capacity recovery phenomenon observed during the capacity degradation of lithium-ion batteries, Liu et al.[22]used empirical mode decomposition (EMD) to decompose raw capacity data into intrinsic mode functions (IMFs) and residuals. These components were then predicted separately, which improved prediction accuracy. The EMD method is prone to mode aliasing, which reduces the accuracy of subsequent predictions[23,24]. The introduction of the Variational Mode Decomposition (VMD) method not only resolves mode aliasing but also addresses the randomness and nonlinearity inherent in capacity data. Combining VMD with a Temporal Convolutional Network (TCN) can reduce data complexity and effectively extract temporal information.

In summary, this paper proposes a method for the joint prediction of lithium-ion battery RUL based on VMD and a multi-scale TCN. The method leverages multi-scale temporal information from both capacity and operational data to enhance prediction.

2. EXPERIMENTAL DATA FEATURE EXTRACTION

2.1 Experimental Data

This study utilizes a lithium-ion battery aging dataset from NASA. The analysis focuses on four 18650 lithium-ion batteries (B005, B006, B007, and B018), each with a nominal capacity of 2 Ah. The data were collected from charge-discharge experiments conducted at a constant ambient temperature of 24°C. In these experiments, the batteries are first charged at a constant current of 1.5 A until the voltage reaches 4.2 V. Then, the charging process switches to a constant voltage mode until the current drops to 20 mA. Discharge is performed at a constant current of 2.0 A until the battery-specific cut-off voltage is reached. The cut-off voltages for B005, B006, B007, and B018 are 2.7 V, 2.5 V, 2.2 V, and 2.5 V, respectively.

During the cycling process, data such as battery current, voltage, temperature, and capacity are measured. Impedance is also measured after the system stabilizes. Since capacity data directly reflects the battery's aging state and remaining useful life, it is adopted as the prediction target in this experiment. The capacity data for the four batteries are shown in Figure 1.

As shown in Figure 1, each battery exhibited varying degrees of capacity recovery. This phenomenon occurs because after a period of rest, the internal chemical processes and structure of lithium-ion batteries can readjust and gradually recover, leading to a slight restoration of performance[25]. Additionally, the initial capacities of the batteries differed, and the test for Battery B018 concluded at the 132nd cycle, whereas the tests for the other three batteries ended at the 168th cycle.

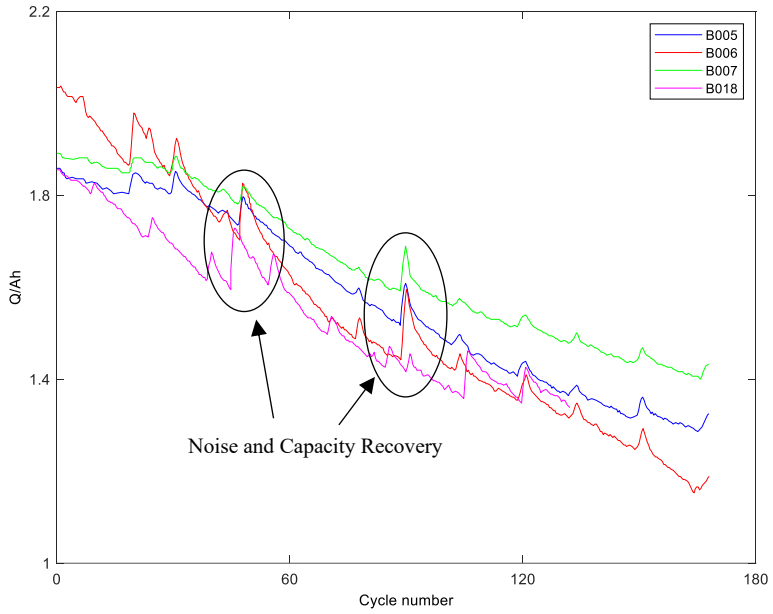


Fig.1 Battery capacity decline curves

2.2 Feature Extraction

The single charge-discharge curves for battery B005 are shown in Figure 2.

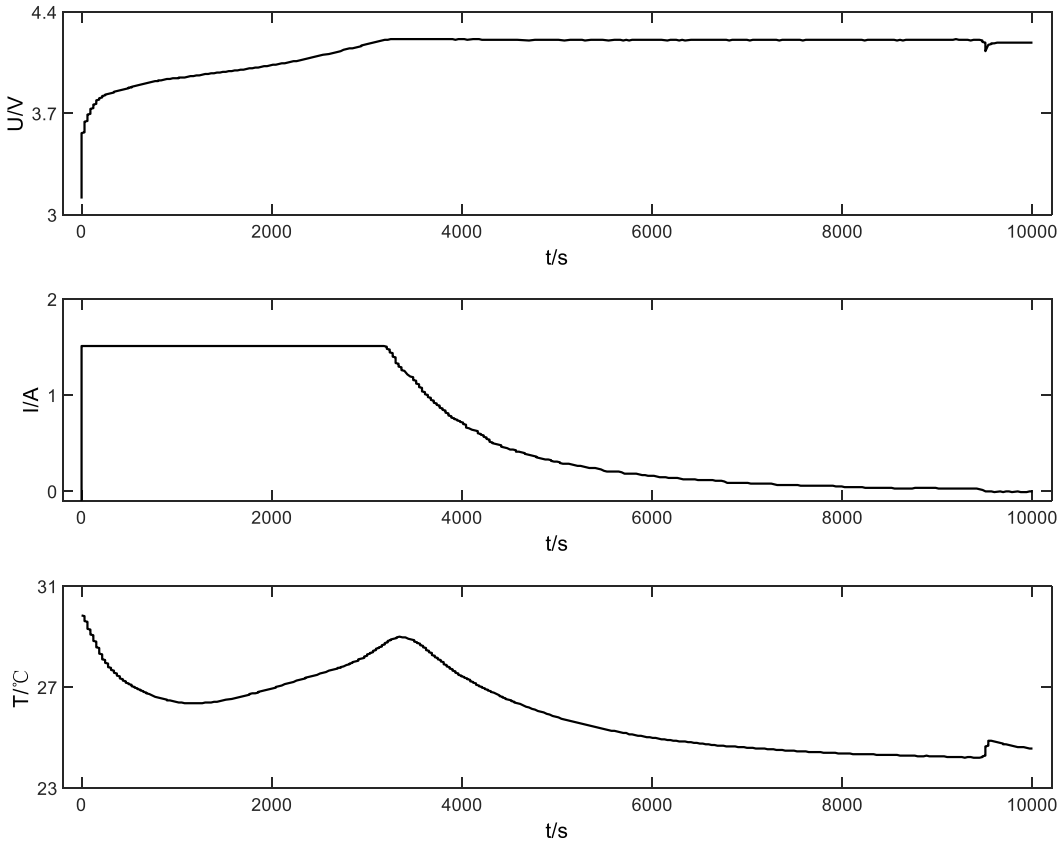


Fig.2 Single charge-discharge curves for battery B005

Twelve features were extracted from the voltage, current, and temperature data. These features can be categorized into three groups:

(1) **Charging Time Features:** the duration of the constant current (CC) charging phase (H1) and the constant voltage (CV) charging phase (H2); the ratio H1/H2; and the total charging time (H1 + H2).

(2) **Cumulative Measures:** the time-integrated current (C1) and temperature (T1) during the CC phase; the time-integrated current (C2) and temperature (T2) during the CV phase; and the total time-integrated current (C) and temperature (T) over the entire charging process.

(3) **Slope Features:** the maximum slopes of the charging voltage (K1) and current (K2) curves.

To mitigate the impact of differing dimensional scales, the features were normalized using the min-max normalization method, which maps the data to the range [0, 1], as shown in Equation (1):

$$x' = \frac{x - x_{min}}{x_{max} - x_{min}} \quad (1)$$

In equation (1): x denotes the original value, while x′ denotes the mapped value.

3. PRINCIPLES OF JOINT PREDICTION METHOD

For the purpose of predicting the RUL of lithium-ion batteries, the capacity data was first decomposed into high-frequency fluctuation components and low-frequency trend components using variational mode decomposition (VMD). Subsequently, a multiscale TCN was applied to predict these components separately.

3.1 The Variational Mode Decomposition Method

The Variational Mode Decomposition (VMD) method is a non-recursive, adaptive signal processing technique that decomposes an original signal f(t) into K band-limited intrinsic mode functions (IMFs)[26]. Compared to Empirical Mode Decomposition (EMD), VMD mitigates endpoint effects and mode mixing, thereby effectively reducing the non-stationarity of the time series[27].

The decomposition is achieved by solving a constrained variational problem. The objective is to ensure that each decomposed mode is a compacted around a central frequency while minimizing the sum of the estimated bandwidths of all modes, under the constraint that the sum of all modes equals the original signal. The corresponding formulation is:

$$\begin{cases} \min\limits_{\{u_k\},\{\omega_k\}} \left\{ \sum_{k=1}^{K} \left\| \partial_t \left[\left(\delta(t) + \frac{j}{\pi t}\right) * u_k(t) \right] e^{-j\omega kt} \right\|_2^2 \right\} \\ s.t. \sum_{k=1}^{K} u_k(t) = x(t) \end{cases} \quad (2)$$

In Equation (2): $\{u_k\}$ represents the set of all intrinsic mode functions (IMFs), $\{\omega_k\}$ is the set of their respective center frequencies, $\delta(t)$ is the Dirac delta function, j is the imaginary unit, $*$ denotes convolution, K is the total number of IMFs, k refers to the k-th mode in the set, and x(t) is the original signal over time t.

By introducing a penalty factor α and a Lagrange multiplier λ(t), the constrained variational problem is transformed into an unconstrained one. This yields the following augmented Lagrangian function:

$$L[\{u_k\},\{\omega_k\},\lambda] = \alpha \sum_{k=1}^{K} \left\| \partial_t \left[\left(\delta(t) + \frac{j}{\pi t}\right) * u_k(t) \right] e^{-j\omega kt} \right\|_2^2 + \|x(t) - \sum_{k=1}^{K} u_k(t)\|_2^2 + \langle \lambda(t), x(t) - \sum_{k=1}^{K} u_k(t) \rangle \quad (3)$$

The Alternating Direction Method of Multipliers (ADMM) is employed to iteratively update u_k^{n+1}, ω_k^{n+1}, and λ using Equations (4) to (6). The iterations continue until the convergence criterion is met, at which point the optimal solution to the variational problem is considered found.

$$\hat{u}_k^{n+1}(\omega) = \frac{\hat{x}(\omega) - \sum_{i \neq k} \hat{u}_i^n(\omega) + \frac{\hat{\lambda}_n(\omega)}{2}}{1 + 2\alpha(\omega - \omega_k^n)^2} \quad (4)$$

$$\omega_k^{n+1} = \frac{\int_0^\infty \omega |\hat{u}_k^{n+1}(\omega)|^2 dw}{\int_0^\infty |\hat{u}_k^{n+1}(\omega)|^2 dw} \quad (5)$$

$$\hat{\lambda}^{n+1}(\omega) = \hat{\lambda}^n(\omega) + \tau[\hat{x}(\omega) - \sum_k \hat{u}_k^{n+1}(\omega)] \quad (6)$$

In Equations (4) – (6): n denotes the number of iterations, τ is the update factor.

The iteration process halts when either the maximum number of iterations is reached or the stopping criterion, defined in Equation (7), is satisfied.

$$\frac{\sum_k \|\hat{u}_k^{n+1} - \hat{u}_k^n\|_2^2}{\|\hat{u}_k^n\|_2^2} < \varepsilon \qquad (7)$$

In equation (7): ε is the relative convergence tolerance, which is approximately 0.

Using battery B005 as a case study, the raw capacity data was decomposed by the VMD method into four components: one low-frequency component (IMF1) and three high-frequency components (IMF2-IMF4), as illustrated in Figure 3.

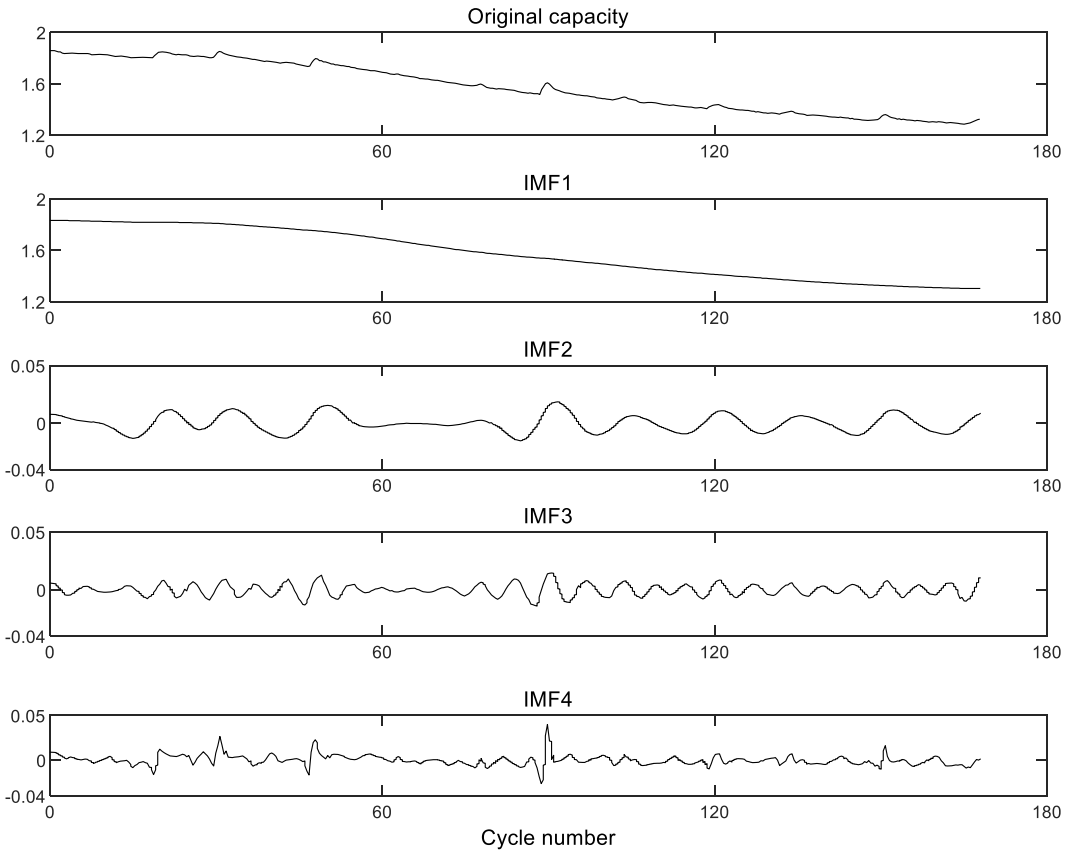


Fig.3 Decomposed high and low frequency components

3.2 Multiscale TCN

The Temporal Convolutional Network (TCN) is a specialized architecture for sequence modeling that enforces temporal causality[28,29]. It effectively captures temporal dependencies within data, enabling the prediction of future values. To maintain this causality while expanding the network's receptive field, TCN utilizes dilated causal convolutions. This technique allows the model to incorporate information from an exponentially growing range of historical data points. Formally, given a 1D input sequence $x \in R^n$ and a filter f:{0,1,⋯,k-1}→R, the output F(s) of the dilated convolution at sequence element s is defined by Equation (8).

$$F(s) = (x *_d f)(s) = \sum_{i=0}^{k-1} f(i) \cdot x_{s-d \cdot i} \qquad (8)$$

In Equation (8): k denotes the filter size, $*_d$ represents dilated convolution, and d is the dilation factor.

Additionally, each layer in the TCN utilizes a standard residual block for feature extraction, as illustrated in Figure 4, with the ReLU function serving as the activation function.

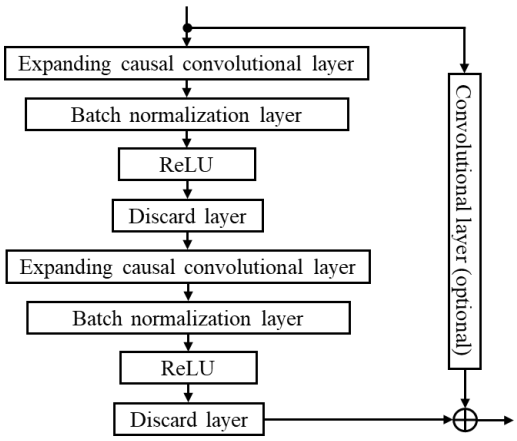


Fig.4 Residual block structure of TCN

The capacity degradation of lithium-ion batteries results from the combined effects of multiple factors over time[30], leading to multi-scale temporal characteristics in the capacity data. Furthermore, the underlying patterns within the collected data are often obscured by noise. To more effectively extract temporal features, convolutional kernels of varying scales were employed to capture multi-scale temporal dependencies. A multi-scale TCN was constructed through parallel learning, with its architecture shown in Figure 5.

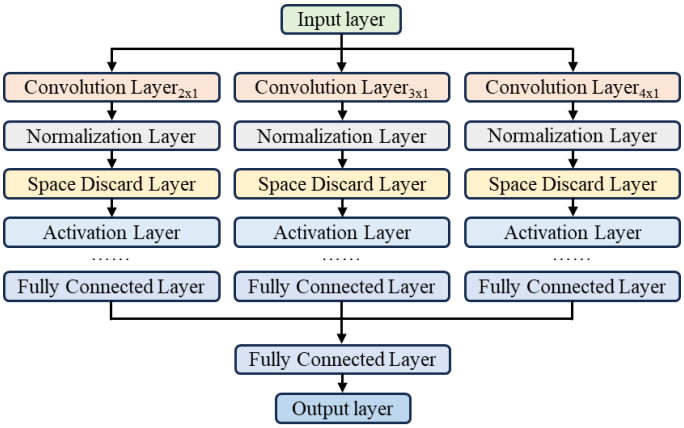


Fig.5 Structure of multiscale TCN

Following parallel learning across multiple scales, the extracted features from each scale were fused and fed into a fully connected layer. The final output was then produced by a regression layer.

3.3 RUL Prediction Process

Due to the nonlinear degradation trend of capacity data, directly applying rolling forecasts to it can lead to state saturation and lag issues in the multiscale TCN. Conversely, relying solely on feature data for capacity prediction makes the model susceptible to noise and the capacity recovery phenomenon, resulting in either underfitting or overfitting. To mitigate these issues, this paper integrates both capacity data and feature data for capacity prediction, which is then used to calculate the RUL. The overall prediction framework based on the multiscale TCN is illustrated in Figure 6.

The implementation process consists of the following steps:

(1) Decompose the battery capacity data into high-frequency (HF) components and low-frequency (LF) components. The HF components capture short-term capacity fluctuations, while the LF components delineate the long-term capacity degradation trend. Both components are then split into training and testing sets of equal size.

(2) Extract health features from operational data (voltage, current, temperature) to characterize the battery's status. Similarly, partition this feature data into training and testing sets, maintaining the same ratio as used for the capacity data.

(3) Training Phase: For the HF components, train a model that takes historical capacity data as input and predicts the subsequent value. For the LF components, train a model that takes the extracted features as input and predicts the LF

component value.

(4) Prediction Phase: For the HF components, employ an iterative forecasting method. For the LF components, input the test-set feature data into its trained model to obtain predictions.

(5) RUL Calculation: Reconstruct the final capacity prediction by combining the HF and LF predictions. The RUL value is then calculated as the number of cycles from the start of prediction until the reconstructed capacity trajectory crosses the predefined failure threshold.

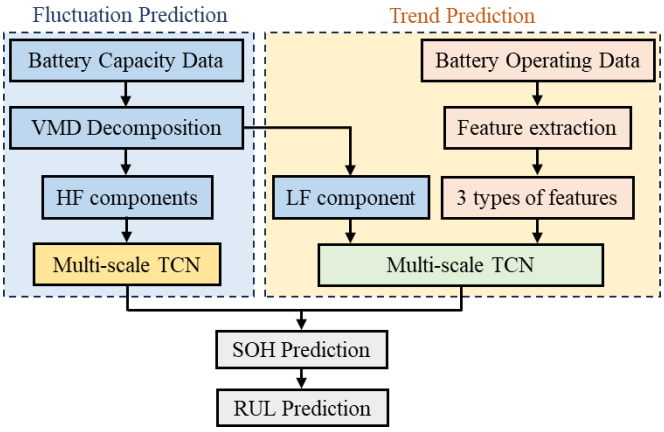


Fig.6 RUL prediction framework by multiscale TCN

4. EXPERIMENTAL VERIFICATION

To validate the effectiveness of the proposed algorithm, RUL prediction was performed based on the NASA dataset.

4.1 Evaluation Indicators

It is generally accepted that when a battery's full-charge capacity drops to 70% of its initial rated value, it can be considered to have reached the end of its service life. The RUL calculation formula for lithium-ion batteries is as follows:

$$N_{RUL} = N_{EOL} - N_{ECL} \quad (9)$$

In Equation (9): N_{RUL} represents the battery's RUL, i.e., the number of cycles remaining before the battery reaches its failure threshold. N_{EOL} denotes the cycle count at which the battery reaches its failure threshold. N_{ECL} indicates the cycle count at the start of the prediction, i.e., the number of cycles the battery has already undergone.

To comprehensively and objectively analyze the validity and accuracy of the capacity prediction results, the performance of the proposed algorithm was evaluated using root mean square error (RMSE) and mean absolute error (MAE), as shown in Equations (10) and (11). The smaller the RMSE and MAE, the more accurate the prediction results.

$$RMSE = \sqrt{\frac{1}{N}\sum_{i=1}^{N}(\hat{y}_i - y_i)^2} \quad (10)$$

$$MAE = \frac{1}{N}\sum_{i=1}^{N}|\hat{y}_i - y_i| \quad (11)$$

In above Equations: $\hat{y}_i$ denotes the predicted value, y_i denotes the actual value, and N denotes the number of data points.

To compare the difference between the actual RUL and the predicted RUL, the RUL prediction absolute error (AE) is defined as shown in Equation (12):

$$AE = \left|N_{RUL} - \hat{N}_{RUL}\right| \quad (12)$$

In Equation (12): N_{RUL} and $\hat{N}_{RUL}$ represent the actual value and predicted value of RUL, respectively.

4.2 Prediction Results and Analysis

To validate the prediction accuracy of low-frequency and high-frequency components, taking battery B005 as an example, different prediction start points N_{ECL} were set within the 50%–70% range of the maximum cycle count. The RMSE and MAE for each decomposed component are shown in Table 1, where IMF1 denotes the low-frequency component and IMF2–IMF4 denote the corresponding high-frequency components.

Table 1 Component prediction error of battery B005

Components	N_{ECL}	RMSE	MAE	Components	N_{ECL}	RMSE	MAE
IMF1	80	0.0322	0.0271	IMF3	80	0.0078	0.0066
	90	0.0281	0.0184		90	0.0084	0.0068
	100	0.0145	0.0113		100	0.0044	0.0037
	110	0.0133	0.0101		110	0.0048	0.0041
IMF2	80	0.0123	0.0100	IMF4	80	0.0057	0.0047
	90	0.0071	0.0051		90	0.0058	0.0046
	100	0.0042	0.0028		100	0.0043	0.0036
	110	0.0047	0.0034		110	0.0047	0.0040

As shown in Table 1, the prediction errors for the three high-frequency components are relatively small, while the low-frequency components exhibit relatively larger errors. This is primarily because: low-frequency components represent trends obtained through decomposition, making them smoother; the decay rate of low-frequency components slows progressively, leading to model underfitting. Furthermore, as the training data increases, both the high-frequency and low-frequency components exhibit decreasing prediction errors, indicating that expanding the training dataset enhances prediction accuracy.

To validate the overall prediction performance of the proposed method, the overall capacity prediction errors for the four batteries were calculated sequentially. The results are shown in Table 2.

Table 2 Capacity prediction error of four batteries

Battery	N_{ECL}	RMSE	MAE	Battery	N_{ECL}	RMSE	MAE
B005	80	0.0356	0.0288	B007	80	0.0370	0.0295
	90	0.0272	0.0178		90	0.0360	0.0271
	100	0.0130	0.0096		100	0.0206	0.0180
	110	0.0111	0.0086		110	0.0104	0.0084
B006	80	0.0688	0.0594	B018	80	0.0255	0.0202
	90	0.0430	0.0332		90	0.0251	0.0200
	100	0.0273	0.0220		100	0.0218	0.0172
	110	0.0243	0.0185		110	-	-

In Table 2, the battery B018 has a maximum cycle count of 132, and its maximum value for N_{ECL} was set to 100, which differs slightly from the other batteries. From a battery perspective, under different prediction starting points, battery B006 exhibited the highest RMSE and MAE. This aligns with the maximum capacity recovery observed for battery B006 in Figure 1, indicating that capacity recovery negatively impacts capacity prediction. From the perspective of N_{ECL}, as the amount of training data increases, the prediction error for the four batteries decreases accordingly.

The SOH failure threshold for lithium-ion batteries is typically set at 70% of the initial state. Based on the predicted capacity data, the absolute error (AE) of RUL prediction for the four batteries are shown in Table 3.

Table 3 RUL prediction error of four batteries

N_{ECL}	B005	B006	B007	B018
80	6	6	-	2
90	2	1	-	0
100	1	1	-	-
110	1	-	-	-

As shown in Table 3: B007 exhibited the slowest degradation rate, with its capacity remaining above the threshold even at the conclusion of the measurement; B018 demonstrated the fastest degradation rate, reaching end-of-life before

N_{ECL} reached 100; B005 showed a moderate degradation rate. The RUL prediction results for battery B005 under different prediction starting points N_{ECL} are shown in Figure 7.

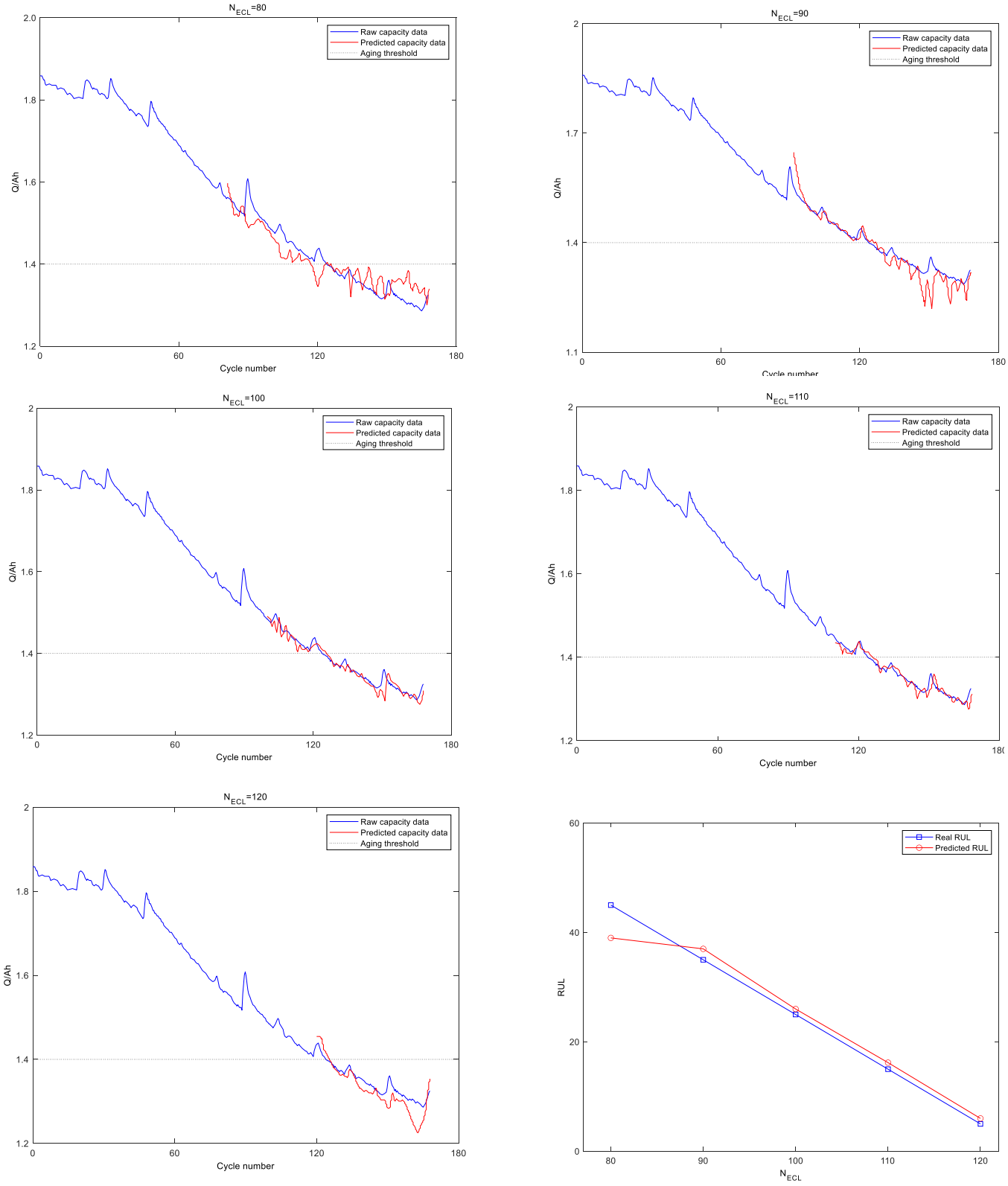


Fig. 7 RUL prediction results of battery B005

As shown in Figure 7: when N_{ECL} values are 100 and 110, the prediction performance is optimal , with the predicted

trend aligning closely with actual capacity and exhibiting minimal fluctuation. When N_{ECL} values are 80 and 90, the prediction errors are relatively larger. This is attributed to the smaller training dataset, which results in underfitting of the model. Similarly, when N_{ECL} is 120, the prediction error increases because the capacity decay rate has changed and the data has not yet been input into the model for training, resulting in insufficient model fitting.

4.3 Comparison of Prediction Methods

To further demonstrate the advantages of the multi-scale TCN model over the single-scale TCN model, capacity prediction was performed using the prediction framework based on the B006 battery data with the highest capacity recovery rate. The capacity and RUL prediction errors are shown in Table 4.

Table 4 Comparison of Prediction Errors for Battery B006

N_{ECL}	Method	RMSE	MAE	AE	N_{ECL}	Method	RMSE	MAE	AE
80	TCN	0.0725	0.0597	11	100	TCN	0.0304	0.0256	3
	multiscale-TCN	0.0688	0.0594	6		multiscale-TCN	0.0273	0.0220	1
90	TCN	0.0510	0.0449	6	110	TCN	0.0275	0.0220	-
	multiscale-TCN	0.0430	0.0332	1		multiscale-TCN	0.0243	0.0185	-

For battery B006, Table 4 shows that the multiscale TCN model exhibits smaller prediction errors across all three metrics. This indicates its superior ability to identify and utilize key information within the data, thereby yielding predictions closer to actual values. By extracting information across multiple time scales, the multiscale TCN model achieves higher prediction accuracy compared to the standard TCN model.

5. CONCLUSIONS

To mitigate the impact of capacity recovery and noise on RUL prediction of lithium-ion batteries, this paper proposed a joint prediction method based on VMD and a multi-scale TCN. By leveraging both the fluctuation details of battery capacity data and operational data characteristics, the proposed method enhances RUL prediction accuracy. The raw capacity data was first decomposed using VMD. The high-frequency components were predicted via a rolling iteration approach, while the low-frequency components were predicted by establishing a mapping relationship with operational data characteristics. Validation using capacity data from four batteries in the NASA dataset demonstrates the effectiveness of the proposed method.

The results indicate that the prediction errors for high-frequency components are generally small, confirming that the VMD-decomposed components are reasonable, exhibit regular patterns, and are suitable for multi-scale TCN prediction. Similarly, the small prediction errors for low-frequency components suggest that the battery performance degradation rate varies dynamically and that operational data are closely related to the battery's aging state. Overall, the results demonstrate that the multi-scale TCN efficiently extracts hidden temporal information from the data, enabling accurate capacity prediction and precise RUL estimation.

Funding statement

This work was supported by the Jinhua Municipal Science and Technology Bureau, Zhejiang Province, China (Project No. 2025-4-035) and the Special Talent Introduction Program of Zhejiang Technical Institute of Economics, Hangzhou, China (Project No. X2025088).

Data availability statement

All data generated or analyzed during this study are included in this article.

REFERENCES

[1] Lv K, Ma Z Q, Bao C J L H, et al. Indirect Prediction of Lithium-Ion Battery RUL Based on CEEMDAN and CNN-BiGRU[J]. *energies*, 2024, 17: 1704.

[2] Zhang J S, Huang C S, Chow M Y, et al. A Data-model Interactive Remaining Useful Life Prediction Approach of Lithium-ion Batteries Based on PF-BiGRU-TSAM[J]. *IEEE TRANSACTIONS ON INDUSTRIAL INFORMATICS*, 2024, 20(2): 1144-1154.

[3] He N, Zhang S Y, Li R X, et al. RUL prediction of lithium battery based on particle filter and GRU neural network fusion[J]. *JOURNAL OF HARBIN INSTITUTE OF TECHNOLOGY,* 2024, 56(5): 142-151.

[4] Yuan N, Mao R Z, Han P H, et al. A dual-exponential EKF model for lithium-ion battery RUL prediction with Bayesian optimization[J]. *Measurement Science and Technology*, 2025, 36(9).

[5] Aljohani A, Aljohani S. A Hybrid GRU-MHA model for accurate battery RUL forecasting with feature selection[J]. *Energy Reports*, 2025, 14: 294-309.

[6] Ye G Z, Feng L, Guo J L, et al. A Simple and Effective KAN-Based Architecture for Accurate Battery RUL Prediction[J]. *IEEE Access*, 2025, 13: 128700-128715.

[7] Jiang F, Han C J, Peng C. Lithium Battery RUL Prediction Method Based on Degradation Model Dynamic Updating[J]. *Lecture Notes in Electrical Engineering*, 2025, 1346:299-306.

[8] Guo X F, Wang K Z, Yao S, et al. RUL prediction of lithium ion battery based on CEEMDAN-CNN BiLSTM model[J]. *Energy Reports*, 2023, 9: 1299-1306.

[9] Wu Z Q, Hu X Y. Prediction of the remaining useful life of lithium-ion battery based on particle filter-long short term memory network[J]. *Proceedings of the Institution of Mechanical Engineers -- Part A -- Power & Energy*, 2025, 239(2): 347-359.

[10] Ahwiadi M, Wang W, An AI-Driven Particle Filter Technology for Battery System State Estimation and RUL Prediction[J]. *batteries*, 2024, 10(12): 437.

[11] Liu Y F, Zhao G Q, Peng X Y. A lithium-ion battery remaining using life prediction method based on multi-kernel relevance vector machine optimized model[J]. *Acta Electronica Sinica*, 2019, 47(6):1285-1292.

[12] Xu J Y, Ma J, Zhang K, et al. A hybrid neural network based on the NARX-BiLSTM for SOH and RUL estimation of power battery[J]. *Ionics*, 2025, 0(0): 1-16.

[13] KHODADADI S K, JIN X, RIZZONI G. Prediction of remaining useful life for a composite electrode lithium ion battery cell using an electrochemical model to estimate the state of health[J]. *J Power Sources*, 2021, 481: 228861.

[14] Bin Y, Yu J M, Zhu Y K, et al. A real-time rain flow algorithm and its application to state of health modeling for LiCoO2 lithium-ion batteries[J]. *Proceedings of the CSEE*, 2017, 37(12): 3627-3635.

[15] Liang H Q, He H W, Dai K W, et al. Research on Lithium Ion Battery Life Prediction Method Based on Empirical Aging Model and Mechanism Model for Electric Vehicles[J]. *Automotive Engineering*, 2023, 45(5): 825-835.

[16] Zhang H, Miao Q, Zhang X, et al. An improved unscented particle filter approach for lithium-ion battery remaining useful life prediction[J]. *Microelectronics Reliability*, 2018, 81: 288-298.

[17] Lan F C, Pan W, Chen J Q. Prediction of Remaining Useful Life of Real-World Vehicle Lithium-Ion Power Battery Based on Aseq2seq-PF[J]. *Automotive Engineering*, 2023, 45(12): 2348-2356.

[18] Chen J Y, Lu Q H, Wang X H, et al. A Lithium-Ion Battery RUL Prediction Method Based on ConvTrans and tAPE Under Capacity Regeneration Noise and Low-Dimensional Time Series Data[J]. *IEEE TRANSACTIONS ON INSTRUMENTATION AND MEASUREMENT*, 2025, 74: 1-14.

[19] Wang P, Fan L F, Cheng Z. A joint state of health and remaining useful life estimation approach for lithium-ion batteries based on health factor parameter[J]. *Proceedings of the CSEE*, 2022, 42(4):1523-1533.

[20] Wu Z Q, Hu X Y, Ma B Y, et al. Prediction of the Remaining Useful Life of Lithium-ion Batteries Based on PF-LSTM[J]. *Acta Metrologica Sinica*, 2023, 44(6): 939-947.

[21] Dong Y C, Pang X Q, Jia J F, et al. Remaining useful life prediction of Iithium-ion batteries based on SVD-SAE-GPR[J]. *Energy Storage Science and Technology*, 2023, 12(4): 1257-1267.

[22] Liu K L, Shang Y L, Ouyang Q, et al. A data-driven approach with uncertainty quantification for predicting future capacities and remaining useful life of lithium-ion battery[J]. *IEEE TRANSACTIONS ON INDUSTRIAL ELECTRONICS*, 2021, 68(4): 3170-3180.

[23] Mao L, Xu J, Chen J J, et al. A LSTM-STW and GS-LM Fusion Method for Lithium-Ion Battery RUL Prediction Based on EEMD[J]. *Energies*, 2020, 13(9): 2380

[24] Liu J, Ma Z Q, Liu G C, et al. Predicting the residual useful life of power batteries based on GRUU-TCN ensemble under multiscale decomposition[J]. *Energy Storage Science and Technology*, 2024, 13(3):1009-1018.

[25] Meng J H, Cai L, Stroe D L, et al. Lithium-ion battery state-of-health estimation in electric vehicle using optimized partial charging voltage profiles[J]. *Energy*, 2019, 185:1054-1062.

[26] Huang Y P, Qi X M, Cheng Y, et al. Prediction of sandstone porosity in coal seam roof based on variable mode decomposition and random forest method[J]. *APPLIED GEOPHYSICS*, 2025, 22(1): 197-208.

[27] Wan J C, Zeng X W, Li J C. Fault diagnosis for gearbox based on parameter optimization VMD combined with wide convolutional neural network[J]. *ELECTRONICMEASUREMENTTECHNOLOGY*, 2025, 48(10): 25-32.

[28] Li B, Lu M Z. Short-Term load forecasting modeling of regional power grid considering real-time meteorological coupling effect[J]. *Automation of Electric Power Systems*, 2020, 44(17): 60-68.

[29] Wang Y Y, Chen J, Chen X Q, et al. Short-Term Load Forecasting for Industrial Customers Based on TCN-LightGBM[J]. *IEEE TRANSACTIONS ON POWER SYSTEMS*, 2021, 36(3): 1984-1997.

[30] Wang J G, Zhang S D, Li C Y, et al. A Data-Driven Method With Mode Decomposition Mechanism for Remaining Useful Life Prediction of Lithium-Ion Batteries[J]. *IEEE Transactions on Power Electronics*, 2022, 37(11): 13684-13695.